APPLIED RESEARCH

Experimental Investigation of the Effect of Conductor Temperature on Corona Performance in Overhead Transmission Lines

KAYUMBA G. ILUNGA[1], **ANDREW G. SWANSON**[1],
NELSON MUTATINA IJUMBA[2], **(Senior Member, IEEE), AND ROBERT STEPHEN**[1]
[1]Department of Electrical, Electronic and Computer Engineering, University of KwaZulu Natal, Durban 4041, South Africa
[2]African Centre of Excellence in Energy for Sustainable Development, University of Rwanda, Kigali, Rwanda

Corresponding author: Kayumba G. Ilunga (grace13or@gmail.com)

ABSTRACT The maximum conductor temperature regulates the maximum amount of power that overhead lines can transmit. Excessive line sag and accelerated conductor ageing may occur if this maximum temperature is exceeded. This is particularly true for the most popular steel-reinforced conductors or aluminium anneals, in which high temperatures can cause grease, which is used to prevent corrosion from seeping. High-temperature low-sag conductors have been developed to increase current carrying capacity. In addition to the temperature constraint, overhead transmission lines largely depend on the corona discharge performance. This paper presents experimental results on the investigation of corona performance due to conductor temperature. An experimental configuration that uses a 10 kVA power transformer in cascade with a 10 kVA high current low voltage transformer both connected to the conductor in the corona cage was successfully developed. This configuration allows for heating the conductor while connected to the high voltage and allows for measuring corona current using the screened electrode method of corona cage. The results indicate an increase in corona current with rising conductor temperature, accompanied by a 25% to 32% decrease in inception voltage. The primary factors contributing to these trends were identified as relative air density and the Townsend coefficient. A temperature model incorporating the ionization region was developed to calculate the relative air density accurately. Additionally, To account for the effect of conductor temperature, the well-known surface inception field strength formula proposed by Peek was refined through optimization. Comparisons between the refined Peek's formula and the measured results demonstrated successful alignment. This research enhances our understanding of corona performance with conductor temperature, providing valuable insights for optimizing transmission line design and operation.

INDEX TERMS Conductor temperature, corona discharge, inception voltage, ionization radius.

I. INTRODUCTION

The demand for uninterrupted power supply is growing due to rapid industrialization and economic growth in South Africa. To meet this demand, it is crucial to enhance and optimize the current carrying capacity of overhead transmission lines. While aluminium conductor steel reinforced (ACSR) is a

The associate editor coordinating the review of this manuscript and approving it for publication was Yuh-Shyan Hwang.

typical conductor used for most power transmission lines, its current carrying capacity is limited because it can only operate at temperatures up to 100°C. The reconductoring of existing lines with High-Temperature Low Sag (HTLS) conductors is proposed to address this limitation and provide a cost-effective and simple solution. These HTLS conductors have a higher power delivery capacity and can operate at temperatures as high as 250°C. This upgrade will significantly increase the current carrying capacity of the transmission lines.

Furthermore, an important aspect to consider is corona discharge, which is an undesirable effect on transmission lines. This research aims to understand how the change in conductor temperature affects corona performance using the corona cage method. By studying this relationship, valuable insights can be gained into how conductor temperature affects corona discharge and its impact on transmission line design.

Corona is an ionization process created in the air by the acceleration of free electrons due to a strong non-uniform electric field. This phenomenon causes radio interference, audible noise, corona loss, and damage to the insulation of electrical equipment [1], [2]. A Corona discharge occurs in a small high-field intensity region near the conductor surface of the transmission line. Considering the microscopic aspect of the discharge, various particles, such as free electrons, ionic species, and excited particles, are created during the corona process in air. Those created particles lead to complex physics and chemical reactions [3]. A better knowledge of the physical and chemical mechanisms of the discharge is necessary to solve various engineering problems [4]. However, despite the complexity of the physicochemical mechanisms of corona discharges, Successful experiments have been designed and performed to verify models of the physicomechanisms of corona [5]. The investigations done by theory, numerical simulations, or experiments on corona discharges have pointed out the influence of the geometrical, atmospheric conditions, electrical characteristics, hydrodynamic parameters, and plasma properties on corona [6]. Therefore, accurate measurements of corona characteristics such as corona pulses, radio interference, and audible noises are important for a better understanding of the discharge. For a particular voltage system, parameters such as conductor geometry, line geometry, conductor surface condition, weather, and atmospheric conditions affect the corona performance. So, before designing transmission lines, examining them under different weather conditions is essential.

Several researchers have investigated the effect of parameters such as pressure, humidity and temperature on corona discharge [7], [8], [9]. The study conducted on corona as a function of temperature is critical because it provides useful independent variables when investigating voltage-current characteristics and the breakdown process [10]. This research looks at corona formation in air at high conductor temperatures in a relatively non-uniform coaxial cylinder configuration.

The coaxial cylinder configuration, also known as a corona cage, has been a frequent electrode arrangement used to study corona discharges. The configuration involves an outer cylindrical cage around a single conductor [11]. There are two ways to measure corona current using the corona cage, one is by feeding the conductor in the cage with high voltage and measuring the current from the grounded cage. The second way is to energize the cage with high voltage and measure the corona from the grounded conductor [12], [13], [14].

In their work on the investigation of conductor temperature effect on power lines corona, Holtzhausen et al. used the corona cage to evaluate the effect of conductor temperature on corona. they considered a temperature range from 20°C to 70°C; their configuration involved preheating the conductor in the cage with an injection transformer before connecting the high-voltage supply. The method was not ideal because the conductor cools down quickly as soon as the current source is disconnected [15]. Pieterse developed an inverted cage configuration method to investigate the effect of conductor temperature on corona. The method consisted of connecting the outside surface of the cage to the high voltage, and the conductor was grounded and connected to the high-current source for heating purposes. The inverted configuration allows precise control of temperature, but the corona can only be measured through a high-voltage coupling capacitor connected to the conductor. This method prohibits the use of screened electrode measurements [16], [17]. Liu et al. investigated the effect of conductor heating and configuration on ozone emission; they developed a configuration where the current source and the high-voltage source were connected to the conductor at the same time. It was stated that a custom-made transformer was used for high voltage, and the current was supplied by a 1:1 transformer with high voltage isolation. No details were provided on the current transformer's isolation method to the high-voltage source [18]. This paper presents an arrangement that employs a cascade transformer configuration connected to the conductor in the corona cage. Our method maintains the temperature of the conductor and enables corona measurement without the need for a coupling capacitor.

This paper's contribution is identifying the corona inception due to the heating of the conductor at temperatures expected for a High-Temperature Low Sag conductor (HTLS) and developing a model that demonstrates that the conductor temperature can be included in the inception strength criteria.

Section I serves as the introduction. Section II delves into the theory of corona discharge. Section III offers details on the experimental setup. Section IV outlines the specific experimental procedures and measurements. Section V presents the results and discussions. Finally, Section VI encapsulates the conclusion.

II. CORONA DISCHARGE THEORY

Corona discharges appear in various forms, determined by field polarity and electrode configurations. They are classified as positive, negative, or AC based on the polarity of the active electrode. Under alternating voltage (AC), the discharge exhibits self-repetitive behaviour, combining both positive and negative corona phenomena. The discharge process under AC differs from that under DC primarily due to residual space charge with the same polarity as the previous half cycle before the onset of corona in the current half cycle. Despite this distinction, the corona modes in each half-cycle closely resemble those observed under direct voltages of the same polarity. The work presented in this paper has focused

on AC corona discharge [19]. Positive corona discharge occurs when the conductor is at a positive potential, ionizing the surrounding air and producing a steady, continuous glow with less noise and more uniform discharge. It begins with burst pulse corona and progresses through streamer and glow corona to spark discharge as voltage increases, relying on photo-ionization for propagation. In contrast, negative corona discharge happens when the conductor is at a negative potential, causing intermittent, pulsating discharges with more noise and visible streamers. It starts with Trichel pulse corona and transitions to spark discharge, requiring higher voltage levels and propagating through impact ionization of gas molecules. A cross-sectional diagram of a coaxial corona cage with the various regions indicated is shown in Fig 1.
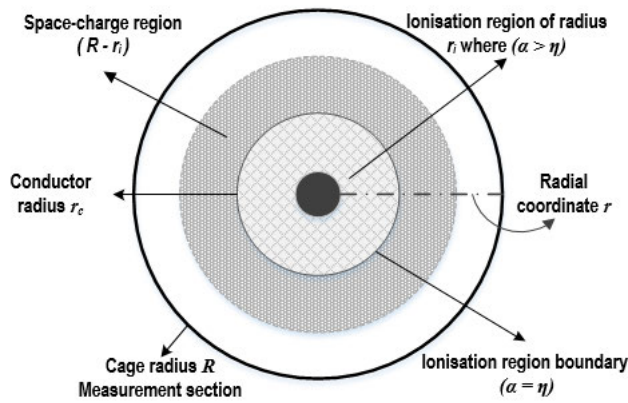

FIGURE 1. Cross-sectional diagram of a corona cage.

When a suitable voltage is applied between the conductor and the cage, high conductor surface electric fields are generated, which are required for corona discharge studies. The discharge space between the two electrodes changes to an ionization zone of radius surrounding the conductor surface of radius r_c and a conduction region of length $(R - r_i)$. The discharge can be separated into two distinct regions: the ionization region, also called the glow discharge region and the drift region or space charges region. The distance from the conductor surface to the inner surface of the cage is called the radial coordinate r, where $r_c \leq r \leq R$. The position where the ionization coefficient equals the attachment coefficient defines the boundary between the two regions. The ionization coefficient α in the ionization region is greater than the attachment coefficient η. As a result, the corona discharge plasma is generated only within this region because of the ionization caused by collisions between free electrons sufficiently accelerated in the electric field and the air molecules [20]. The ionization radius of the corona inception occurs when the conductor surface voltage gradient reaches a critical value. Alongside the conductor diameter and its surface condition, the corona inception gradient depends, as well as on the relative air density, which accounts for pressure and temperature. These dependencies have been investigated and described by approximate expressions

derived experimentally and, to some extent, theoretically in the form of the well-known Peek's empirical formula. The corona inception voltage for the coaxial configuration is given by:

$$V_{inc} = E_i \times r_c \times \ln \frac{R}{r_c} \tag{1}$$

where r_c is the radius of the conductor in cm, R is the radius of the cage in cm, and E_i is the surface inception electric field strength in (kV/cm) and it is given by Peek's formula:

$$E_i = 21 \times m \times \delta \times (1 + \frac{K}{\sqrt{\delta r_c}}) \tag{2}$$

where m is the surface roughness of the conductor, K is constant derived experimentally and δ is the relative air density given by:

$$\delta = \frac{p}{p_o} \times \frac{T_o}{T} \tag{3}$$

where T_o is the standard temperature (K), T is the ambient air temperature (K), p_o is the standard pressure (hPa), and p is the ambient pressure (hPa).

The empirical expression for electric field strength, as presented in equation (2) by Peek, establishes a connection between temperature and corona inception voltage, taking into account the relative air density. The correlation between relative air density and temperature is detailed in equation (3). Notably, an increase in ambient temperature leads to a decrease in relative air density. However, it becomes crucial to ascertain the appropriate temperature for computing the reduced air density between the ambient and conductor temperatures in scenarios involving conductor temperature. When the conductor is electrically heated to a temperature surpassing that of the surrounding air, a temperature gradient emerges across the active ionization zone, resulting in a reduction of the relative air density within the ionization zone. Award and Castle have defined in the equation (4) this temperature gradient as an average temperature and have provided the subsequent relation for relative air density [21]:

$$\delta = \frac{T_0}{T_{av}} \tag{4}$$

where T_o is the absolute temperature of the gas at constant pressure.

The aforementioned representation of relative air density lacks precision regarding the average temperature, particularly concerning its distribution across the radial distance between the two electrodes. This expression finds its appropriateness when space charges generated by corona encompass the entire interelectrode region, as observed in the context of direct current (dc) corona. It is well-established that a primary distinction between DC corona and alternating current (AC) corona lies in space charge distribution [22].

In 1980, Morgan and Morrow conducted a comprehensive experimental investigation into the influence of conductor surface temperature on the occurrence of corona in both alternating current and direct current transmission systems.

Their research revealed that conductor surface temperature significantly influenced the onset of corona in both AC and DC conductors. As a result of their findings, they introduced equation (5) as a valuable and effective parameter for determining the appropriate temperature to be employed in the computation of relative air density, thus contributing to a deeper understanding of corona phenomena in electrical systems [23].

$$T = T_a + 0.8\,(T_s - T_a) \tag{5}$$

where T_a and T_s are, respectively, the ambient and the conductor surface temperatures. The constant 0.8 is a factor determined by experimental analysis and accounts for the temperature gradient of the corona cage. In this manuscript, we have examined the correlation between conductor temperature and the performance characteristics of corona discharges.

III. EXPERIMENTAL SETUP

The experiment was conducted at the High Voltage Direct Current Laboratory on the University of KwaZulu-Natal Westville Campus. Located 160 meters above sea level, the laboratory has an air conditioning system that maintains stable atmospheric conditions. The temperature is regulated between 23°C and 25°C before any experiment. Two sensors placed at different locations monitor the humidity and temperature, allowing for adjustments in case of deviations. The effect of wind speed was neglected, given that the experiment was performed in an indoor cage. The relative humidity and air pressure were stable, respectively, at 55% and 1030 hPa.

Fig 2 illustrates the experimental setup employed in this study, utilizing a coaxial cylinder configuration. The arrangement consisted of a cylindrical outer surface divided into three sections: two guard sections measuring 25 cm each and one central section measuring 50 cm. All sections shared a diameter of 50 cm. The two guard sections of the cylinder were grounded to prevent electromagnetic interference from external sources and connections. To ground the central section of the cylinder, a 1 kΩ resistor was incorporated in series. The resistor was connected to a data acquisition (DAQ) system comprising a picoscope and high-speed computers, facilitating the measurement process.

To facilitate efficient heat conduction, a conductor made of an aluminium alloy tube measuring 120 cm in length and 1 cm in diameter was employed and mounted coaxially inside the cage. The thickness of the tube was 0.1cm. The decision to utilize a tube was based on maximizing the heat generated by the high current.

To capture the visual corona discharge surrounding the corona current measurement system, we employed a camera equipped with an ultraviolet imaging detector; the camera is called a Corocam.

Two types of connections were employed for the experiment; the first type of connection was a typical connection where only the high-voltage source was connected to the
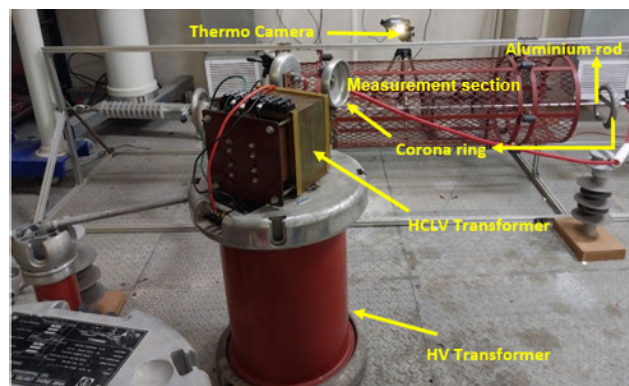

FIGURE 2. Experimental setup.

conductor in the cage. The second type involved a more intricate arrangement, wherein the conductor was simultaneously connected to both the high-voltage transformer and the high-current low-voltage transformer (HCLV) using the secondary low-voltage winding of the cascade transformer. With this method, it is possible to control the conductor temperature simultaneously with the voltage applied to the conductor. The high-current transformer was connected in cascade with the high-voltage transformer. This connection was made to isolate the high-current transformer against high voltage. To achieve this, a tank-type high-voltage transformer rated at 10 kVA with a primary voltage of 220 V and a secondary voltage of 100 kV was used with a high-current low-voltage (HCLV) transformer, also rated at 10 kVA. This transformer features a two-winding primary voltage of 220 V and 330 V, and a secondary voltage of 3.13 V. The rated currents for the HCLV transformer are 45 A and 30 A on the primary side, and 3195 A on the secondary side. The HCLV transformer was placed on top of the HV transformer and maintained at a potential of the output voltage of the HV transformer above the ground. The high-voltage winding of the HV transformer was connected to the magnetic core of the HCLV transformer. The low voltage winding of the primary of the current transformer was supplied from the excitation winding of the HV transformer, which is in series with the high voltage winding of the HV transformer at its high voltage end. Fig 3 displays the schematic of the experimental setup of the HCLV transformer and the HV transformer connected to the corona.

Prior to conducting any experiments, it was crucial to assess the measurement uncertainty. During the connection of the current transformer to the HV transformer on the conductor, significant amounts of noise and corona were observed within the measurement system and setup. Furthermore, a visual corona discharge was noticed on the current HCLV end fitting.

In order to guarantee the absence of undesired corona discharges and disruptions in the setup and measurement system, supplementary corona rings were integrated at the terminal end of the HCLV and along the conductor within the
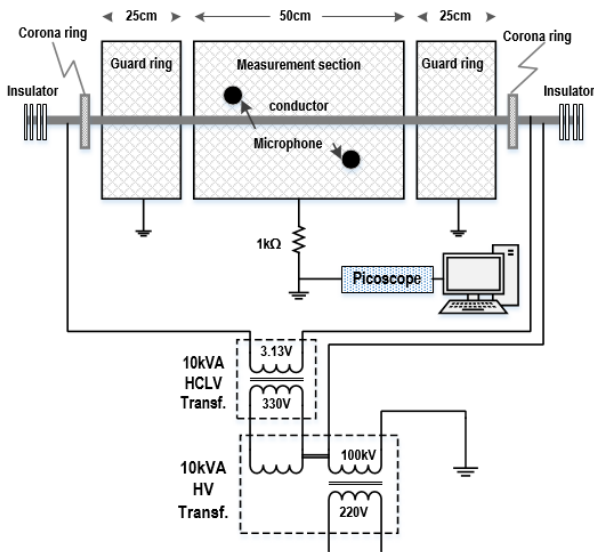
FIGURE 3. Schematic of the experimental setup.

enclosure, as illustrated in Fig 2. This inclusion was intended to alleviate any potential problems associated with noise and corona phenomena. The background noise was measured, and it has been noticed that the outer surface of the cage provides reasonable shielding to the lower frequency range of background noise.

IV. EXPERIMENTAL PROCEDURE AND MEASUREMENT

The procedure consisted of applying first the voltage to the conductor connected to the HV transformer only (ambient measurement). The applied voltage was gradually increased by a step of 5 kV. The corona inception voltage was determined by observing the first occurrence of corona on the Corocam. RMS measurement and the corona pulses were measured using the Picoscope to better quantify the corona current. Two microphones were used for audible noise recording. The experiments were repeated three times to verify the accuracy of the results. The image of the visual corona at ambient temperature measurement is displayed in Fig 4.

FIGURE 4. Visual corona at 45kV for ambient temperature measurement.

The first visual corona was recorded at 45 kV and was considered as the inception voltage for the ambient measurement.

In the second configuration, the conductor was connected to both the HV transformer and the HCLV transformer to enable heating. The HCLV transformer had two available input voltage options: one set at 220 V input and the other at 330 V input.

The inclusion of both 220 V and 330 V connections was considered in this study, as they allowed for a comparative analysis of the conductor's heating behaviour. The higher current achieved at the same voltage in the 220 V connection (Connection 1) resulted in rapid heating of the conductor.
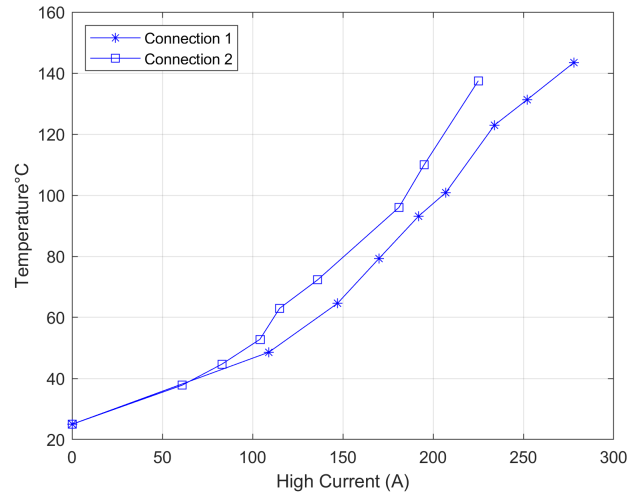

FIGURE 5. Conductor temperature versus conductor (HCLV secondary) current.

Plot 5 illustrates the temperature fluctuation corresponding to the HCLV transformer's secondary current concerning two distinct high-temperature connection configurations. Significantly, the graph clearly demonstrates that when the transformer is linked through the 220 V input (Connection 1), the conductor temperature exceeds that observed when it is connected through the 330 V input (Connection 2) at the same applied voltage. This discrepancy indicates the possibility of achieving different temperatures despite applying an identical voltage.

Fig 6 illustrates the variations in temperature and HCLV secondary current relative to the applied high voltage for two different temperature connections. As shown in the figure, at 55 kV, the measured current is 278 A for connection 1 and 225 A for connection 2. The current density of the conductor at the maximum current was calculated to be 7.38 A/mm^2 for connection 1 and 5.97 A/mm^2 for connection 2.

The procedure was almost the same as for the previous experiment. In addition, the conductor temperature was monitored using a thermal camera. After applying the voltage and the current to the conductor, it was important to wait almost 5 minutes before taking any measurements to allow the conductor temperature to stabilize. The images of the visual corona for the temperature experiment at connection 1 and connection 2 are displayed in Fig 7. the inception voltages
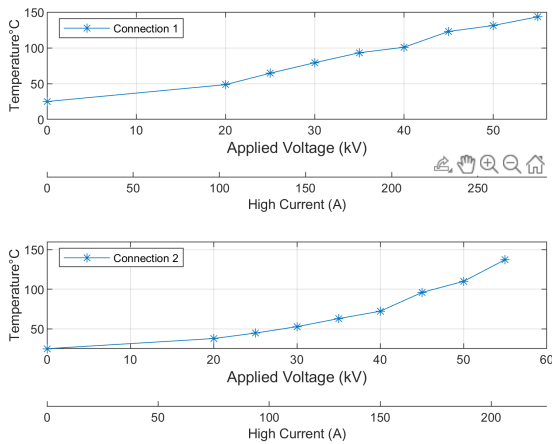
FIGURE 6. Applied voltage (and high current) versus conductor temperature.
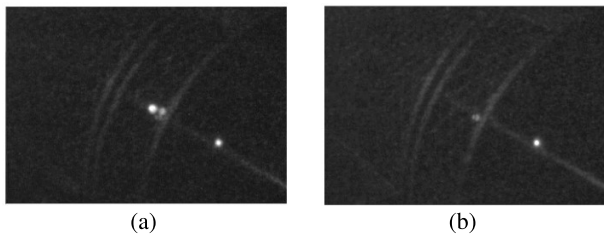

FIGURE 7. Visual corona at 30kV (a) and 32kV (b) for conductor temperature measurements.

for the visual corona were 32 kV and 39 kV, respectively, for connections 1 and 2.

V. RESULTS AND DISCUSSION

The corona pulses, and RMS values for each experimental setup were recorded. A significant temperature increase was observed at 20 kV, and all measurements were made across the voltage range from 20 kV to 60 kV. Notably, visual corona phenomena were observed at 45 kV in the ambient temperature arrangement and around 32 kV to 39 kV for temperature connections 1 and 2. However, an observation emerged that the visual corona might simply be a discharge on the conductor's surface. This conclusion stems from the fact that corona pulses, considered as a more accurate measurement of corona activity, were only detected at higher voltage levels than those associated with the visually observed corona at 45 kV for ambient connection.

Fig 8 shows the images of the visual corona at different applied voltages for ambient conditions (a), connection 1(b), and connection 2(c). The visual corona images clearly show the difference in corona activities around the conductor for different temperatures. As seen in Fig 8, there is more corona around the conductor at the same applied voltage when the transformer is connected at 220V, which corresponds with the highest temperature setup. The measured corona pulses at different voltages and temperatures are displayed in Fig 9.

The first visual corona was observed at 32 kV for connection 1 which corresponds to the conductor temperature of 115°C and for connection 2 it was observed at 39 kV and 99°C. However, the first corona pulses were measured at 35 kV when the HCLV transformer was at connection 1, and the measured temperature was 128°C.

When the HCLV transformer was at connection 2 the first pulses were measured at 43 kV and the conductor temperature was 125°C. The visual corona and the corona pulses measurement results have shown that the corona inception voltage decreases with increased temperature.

The investigation into corona pulse measurements reveals a noteworthy correlation: under identical applied voltage conditions, corona pulse amplitudes exhibit an upward trend as the conductor temperature increases. Moreover, it has been noted that when pulse measurements are conducted at room temperature, with no additional conductor heating, the prevalence of negative corona instances surpasses that of positive corona. In contrast, measurements conducted at elevated temperatures exhibit an increase in both positive and negative corona occurrences. This supports the claim that elevated conductor temperatures amplify alternating current (AC) corona phenomena across both positive and negative amplitudes.

When examining varying voltage scenarios, it becomes evident that the positive corona pulse magnitudes experience a more pronounced temperature-dependent increase than their negative counterparts. This observation can be attributed to the distinctive factors influencing positive and negative corona. Specifically, a positive corona is contingent upon the distribution of ion space charge density near the discharge electrode, whereas a negative corona is influenced by the electric field and its gradient along the outer surface of the conductor. These findings align with the research conducted by Chartier et al., which underscores disparities in electric current density and ion concentration between positive and negative corona phenomena [24].
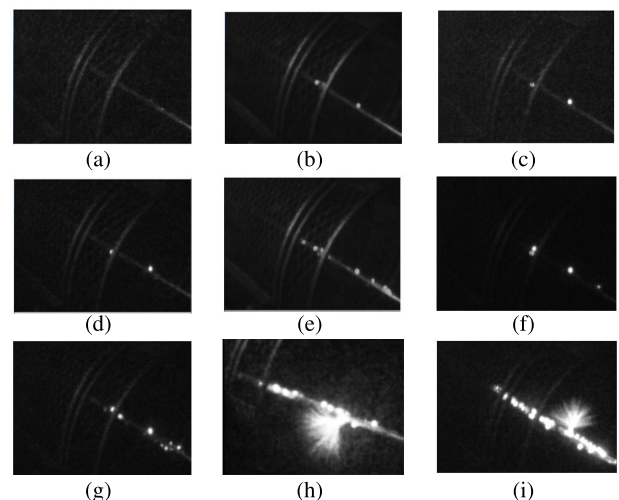

FIGURE 8. Visual corona at 35 kV for different setup configuration (a) Ambient, (b) Connection 1, (c) Connection 2.
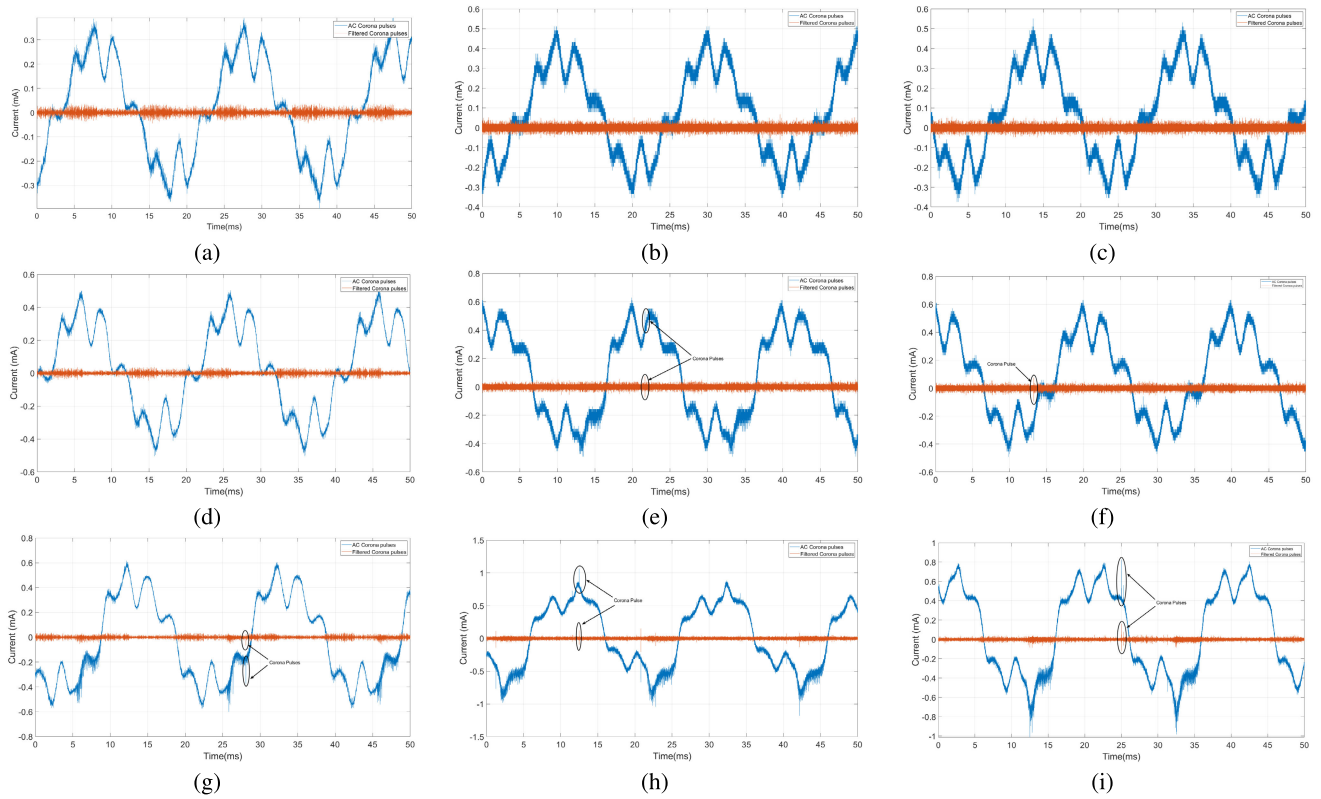
FIGURE 9. Corona Pulses different voltage at 35 kV (a) ambient, (b) Connection 1, (c) Connection 2. At 45 kV (d) ambient, (e) Connection 1, (f) Connection 2. At 55 kV (g) ambient, (h) Connection 1, (i) Connection 2.

Table 1 presents RMS values of the observed corona current. It is evident from these values that as the conductor temperature rises, the magnitude of the corona current also increases.

TABLE 1. RMS values of corona current under different conductor temperatures and applied voltages.

	Applied Voltage (kV)	Temperature (°C)	Corona current (mA)	Audible Noise(dBA)
Ambient	35	24.95	0.171	38.8
	45	24.95	0.225	42.6
	50	24.95	0.285	50.6
T-Con-1	35	117.18	0.246	38.8
	45	155.04	0.314	55.3
	50	176.1	0.410	63.5
T-Con-2	35	99.2	0.248	38.8
	45	128.2	0.293	46
	50	147.8	0.371	57.7

Based on the experimental results, it has been observed that the conductor temperature has a direct impact on both the corona inception voltage and corona activities. As the temperature rises, the corona inception voltage decreases while corona activities increase. For instance, with an increase in temperature from 24°C to 137.9°C, there is almost a 32% decrease in the corona inception voltage. The inception decreases from 49 kV to 37 kV. Similarly, when the temperature rises from 24°C to 142°C, the corona inception voltage decreases from 40 kV to 32 kV, which is almost 25%.

Regarding audible noise, the outcomes reveal a greater amplification associated with elevated temperatures, particularly at higher voltage levels. At 35 kV, the audible noise level remains relatively consistent across all connections. However, at 45 kV and 50 kV, there is a discernible rise in audible noise, amounting to 7% and 20%, respectively. The results indicate a direct correlation between temperature and corona current in the context of corona activities. The tabulated results demonstrate a noticeable escalation in corona current with rising temperatures. Precisely, a temperature increase from 24.95°C to 88.1°C at 35 kV corresponds to a 12% surge in corona current. Similarly, at 50 kV, elevating the temperature from 24°C to 131.3°C results in a more substantial 33.5% increase in corona current.

In the context of alternating current (AC) voltages, the presence of a periodically reversing electric field confines the spatial distribution of space charge generated by AC corona to the immediate vicinity of the conductor. In light of this observation concerning the spatial confinement of space charge in AC corona, it becomes imperative to investigate and quantify the temperature gradient within the ionization region proximal to the coronating area [25]. In this paper, the corona onset in coaxial cylinders can be approximated using Townsend's method (3), where it is assumed that the divergent electric field can be segmented into two distinct regions. In the immediate proximity of the wire, the gas becomes significantly ionized within a radius denoted as r_i, beyond

which the electric field decreases below the critical threshold of 30 kV/cm [15]. Our study focuses on the corona theory, particularly emphasizing the ionization regions around the conductor within the gap between the electrodes. In the coaxial arrangement, the wire of radius r_c forms the high field electrode, and the cage of radius R surrounding the wire forms the low field electrode. If we consider r the radial distance between the centre of the inner electrode and the outer electrode, the electric field strength decreases as a function of r [15]. The electric field that generates corona is higher in the ionization region close to the conductor. Some researchers [15], [16] have experimentally demonstrated that the ionization radius r_i of corona is solely influenced by the discharge wire's radius r_c and remains unaffected by the corona current. Conversely, other researchers [13], through both experimental and theoretical approaches, have found that the ionization radius r_i of corona discharges depends not only on the wire radius r_c but also on the corona current. Despite certain uncertainties and assumptions in its derivation, the equation 6 offered by Combine [26] for calculating the distance r_i at which the field falls below the ionization threshold of 30 kV/cm aligns well with Peek's empirical formula 2.

$$r_i = rc + 0.3\sqrt{rc} \qquad (6)$$

The equation (6) is used in this study to calculate the temperature within the ionization regions. The heating of the conductor leads to a rise in the temperature of the air layer encompassing the conductor. The measured inception electric field was graphed against the conductor temperature to assess the impact of temperature on the corona inception voltage. The measured inception Electric field was derived using the formula described in 1.

$$E_i = \frac{V_{inc}}{r_c \times \ln \frac{R}{r_c}} \qquad (7)$$

where V_inc is the measured corona inception voltage. The parameters r_c and R refer to the conductor and cage radius, respectively, as defined in 1.

Fig 10 illustrates the change in surface inception field strength with temperature. The graph indicates a decrease in surface inception field with an increase in conductor temperature. The temperature influencing the surface inception field strength is situated within the ionization region and differs from the conductor temperature. We have developed a mathematical model based on experimental data to compute this temperature within the ionisation radius. This model aims to determine the temperature required for establishing relative air density. The identified temperature parameter plays a fundamental role in applying the Peek empirical relation, especially in scenarios where conductor temperature is of critical significance.

The approach incorporates a least-squared optimization method strategically utilized to derive a temperature model tailored for precision in air density calculations. The core objective was establishing a mathematical function that
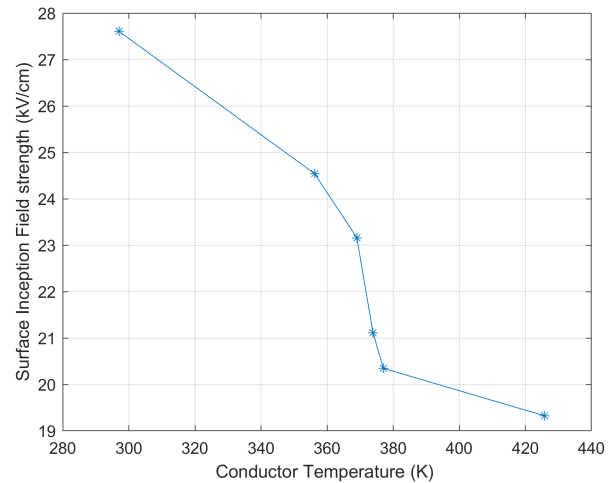

FIGURE 10. Conductor temperature vs measured surface inception field strength.

seamlessly reconciles the measured values obtained through the experiment with Peek's empirical formula. In developing our model, we optimized Peek's formula by utilising sum squared error performance. In our methodology, The temperature in the air density model was substituted with a new model that integrates both conductor temperature and ionization radius, considering constant pressure conditions. This modification enabled the development of an adjusted formula that expresses air density as a function of temperature and corona ionization radius. Incorporating this modification played a crucial role in capturing the complex interaction among these factors, providing a more comprehensive and realistic representation of the system under investigation.

The results obtained through the optimization technique indicate that the temperature within the ionization radius, accounting for the conductor temperature, can be ascertained using the following relation.

$$T_{ri} = T_c \times (1 - A \times e^{-\lambda r_i}) \qquad (8)$$

where: T_{ri} is the temperature within the ionization region of radius r_i, T_c is the conductor temperature the coefficient A and the coefficient λ have been determined and were established at A = 0.7154 and λ = 0.6809.

Moreover, we introduced an additional parameter into the well-established Peek formula. This parameter, determined through experimental analysis, is designed to account for variations in air density and other relevant parameters close to the conductor. By incorporating this empirically derived parameter, we sought to optimize our model's performance further and ensure its applicability across a broader range of conditions. The modified Peek's formula, enriched by the incorporation of the additional constant, is expressed as follows:

$$E_{i\,\text{mod}} = 21 \times m \times \delta \times \left(1 + \frac{K}{\sqrt{\delta r_c}}\right) + \frac{B}{\delta r_c} \qquad (9)$$

where m is equal to 0.8, K is a constant equal to 0.301, δ is the relative air density calculated using the temperature found in (7), B is constant equal to -0.2733,

The temperature model, derived through experimental means, was used to determine the air density. This obtained air density was then employed in relation (9). Subsequently, the calculated inception electric field was graphically plotted against the conductor temperature and was compared to the measured electric field.
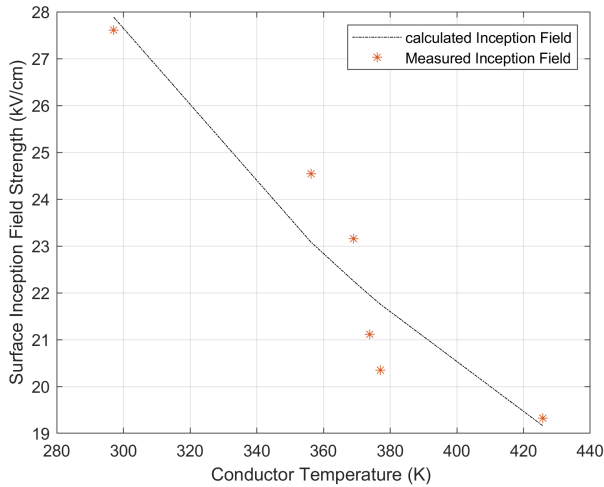

FIGURE 11. Conductor temperature vs measured and calculated surface inception field strength.

The graphical representation Fig 11 reveals that the adjusted formulation adeptly captures the nuanced interaction between conductor temperature and ionization radius, resulting in a more refined and precise depiction of surface inception field strength.

We conducted additional experiments to validate the experimental model using various types of conductors with different cross-sectional characteristics. Specifically, we employed two solid copper tubes with hard-drawn properties, measuring 0.32 cm and 0.46 cm in radius, as well as a soft-drawn copper tube with a radius of 0.36 cm, each with a thickness of 0.1 cm. The selection of copper was justified by its availability and superior heating performance compared to aluminium. These conductors were inserted into the corona cage to broaden the scope of the investigation. The experimental setup and procedural steps remained consistent with the initial configuration throughout these supplementary experiments, ensuring a rigorous and reproducible methodology.

Fig 12 presents the experimental outcomes depicting the relationship between surface inception field strength and conductor temperature for all four conductors, including the aluminium and three copper conductors.

After conducting these additional experiments, we compared the results obtained from the mentioned conductors with the outcomes predicted by the optimized model.
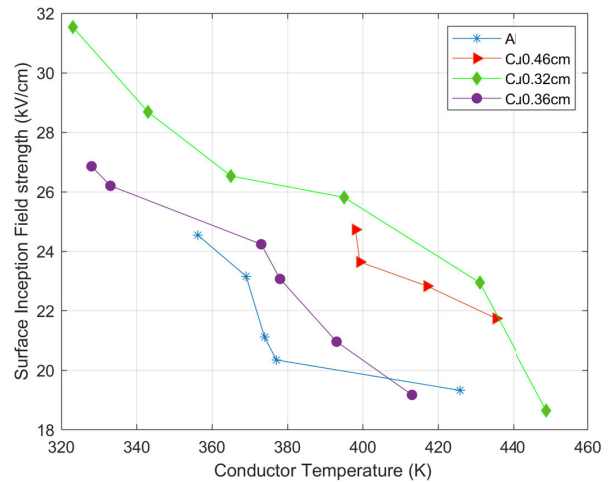

FIGURE 12. Conductor temperature vs surface inception field.

The comparative analysis is visually represented in the subsequent figures.
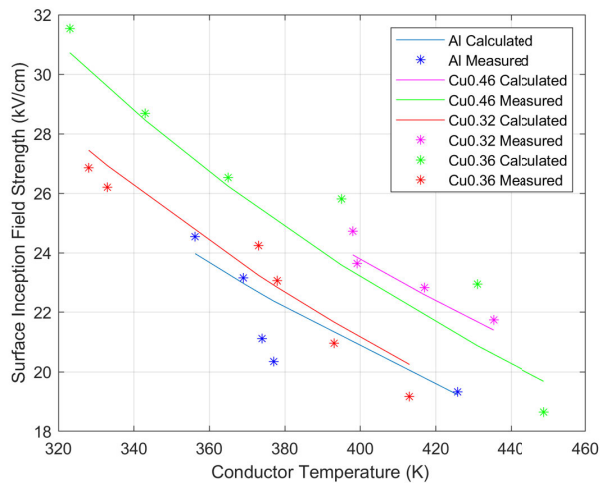

FIGURE 13. Comparison between measured, calculated and optimized Inception Electric field of different conductors.

Upon examination of Fig 12 and Fig 13, a convergence becomes apparent between the experimental data and the predictions formulated by the proposed model. These findings collectively emphasize the model's capability to elucidate the intricate inter-dependencies between corona inception voltage and conductor temperature. The consistent correspondence between the model and experimental observations across diverse conditions confirms the model's accuracy and provides insightful perspectives into the fundamental mechanisms governing corona inception.

A. INFLUENCE OF CONDUCTOR TEMPERATURE ON AUDIBLE NOISE

The audible noise level was plotted against the conductor surface electric field for all conductors and conditions
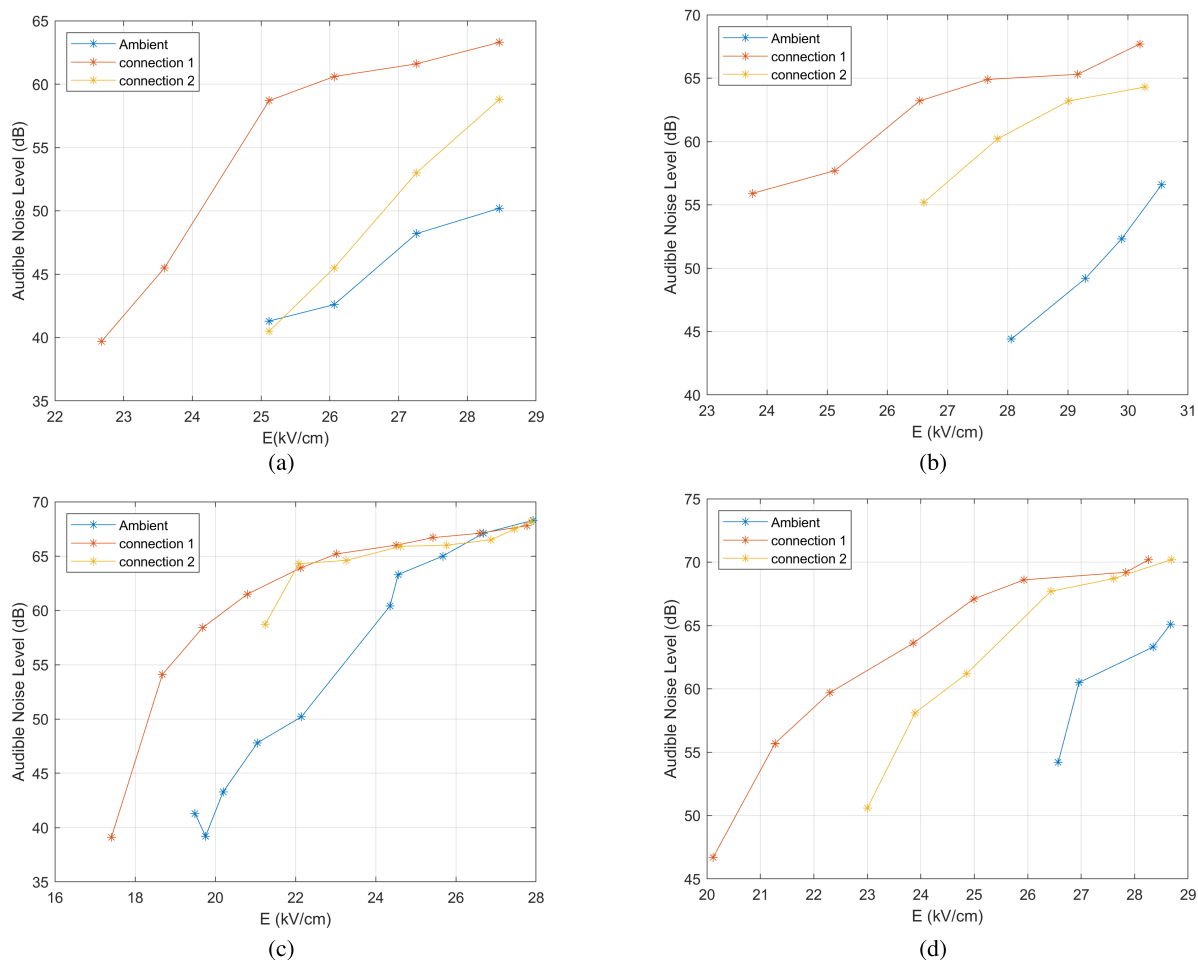
FIGURE 14. Conductor surface electric field vs Audible Noise level for different conductors and conditions, (a) Aluminium conductor, (b) Cu0.46, (c) Cu0.32, (d) Cu0.36.

investigated in this study. The conductor surface electric fields were normalized by air density to mitigate the impact of temperature on the measurements. The subsequent figures illustrate the graphical representation of the conductor surface electric field plotted against the audible noise level.

The results illustrated in Fig 14 indicate a rise in audible noise levels when the conductor is subjected to high temperatures under identical applied voltage for all connections. Additionally, it has been noted that for connections 1 and 2, audible noises commence at lower electric fields than the ambient connection. This signifies an earlier onset of audible noise generation due to high conductor temperature. However, saturation in audible noise is evident in Fig 14(c) for all connections occurring at specific higher conductor surface electric fields. This phenomenon can be attributed to increased corona activities around the conductor due to the smaller radius of the particular conductor.

The increase in corona intensity can be explained by the dependence of Townsend's ionization coefficient α on the intensity of the electric field and the relative air density inside

the ionization region. Townsend's coefficient α, which measures the number of electrons generated over a 1 cm distance travelled in the applied voltage direction by a single electron, rises with increasing electronic energy [27], [28]. High temperature leads to a decrease in the relative air density of the gas mixture, which increases the mean path of the electrons and gas molecules. The free electrons emitted during the initial ionization process are dramatically accelerated and cause the rise of electronic energy. It is also important to consider that increased mobility of ions and electrons at elevated temperatures can further enhance ionization rates, potentially amplifying corona current. The Townsend ionization coefficient increases at higher temperatures. The inelastic collisions between the gas molecules and electrons increase and produce more electrons and positive ion pairs, thus causing a high discharge current at high temperatures [29], [30].

The investigation aimed to understand how the temperature of the conductor affects the corona performance of High-Temperature Low-Sag (HTLS) conductors. Our findings indicate that the inception voltage decreases at temperatures equal to or exceeding 372 K. This temperature range

surpasses the operational voltage of standard Aluminum Conductor Steel Reinforced (ACSR) conductors.

In terms of inception voltage, conductors at high temperatures demonstrate higher corona noise and lower inception. HTLS can function better at higher temperatures than ACSR, and the corona performance of the conductor running at a higher temperature must be accounted for. For instance, examining Table 1 at 50 kV, the corona current is 0.285 A at 297.95 K and increases to 0.371 A at 420.8K. This represents a 30% increase in current for a 41% rise in temperature. This suggests that HTLS performs better in terms of corona discharge under elevated temperatures compared to traditional ACSR conductors.

VI. CONCLUSION

In conclusion, our experimental investigation has provided crucial insights into the intricate relationship between conductor temperature and corona discharge. By utilizing an advanced measurement system that integrates a high-voltage transformer in cascade with a high-current low-voltage transformer, we accurately measured corona current pulses through the use of electrode screen techniques. The consistent findings underscore a direct correlation between conductor temperature and the amplitude of corona current pulses, impacting both peak and root mean square (RMS) values. Notably, we observed a decrease in corona inception voltage as the conductor temperature increased.

Incorporating a theory centred around the corona ionization region has deepened our understanding of how conductor temperature influences corona discharge. It became evident that the temperature within the ionization region, crucial for corona, differs from the overall corona temperature.

Our success in developing a temperature assessment model specifically for the ionization region was pivotal. This model facilitated the determination of the relative air density necessary for Peek's inception field formula, which was further refined through optimization to better align with conductor temperature. The successful comparison of results from this optimized formula with experimental data reinforces the reliability and effectiveness of our approach.

Expanding our focus to include corona audible noise, we explored its relationship with the surface gradient electric field under various conditions. The consistent findings revealed a progressive increase in audible noise with increased conductor temperature, eventually reaching saturation at specific voltage levels. This comprehensive exploration significantly enhances our understanding of the complex interplay between conductor temperature and corona discharge phenomena.

ACKNOWLEDGMENT

REFERENCES

[1] X. Chen, L. Lan, H. Lu, Y. Wang, X. Wen, X. Du, and W. He, "Numerical simulation of trichel pulses of negative DC corona discharge based on a plasma chemical model," *J. Phys. D, Appl. Phys.*, vol. 50, no. 39, Oct. 2017, Art. no. 395202.

[2] F. Yin, M. Farzaneh, and X. Jiang, "Corona investigation of an energized conductor under various weather conditions," *IEEE Trans. Dielectr. Electr. Insul.*, vol. 24, no. 1, pp. 462–470, Feb. 2017.

[3] N. Feng, T. Ma, and C. Chen, "Simulation and study of DC corona discharge characteristics," *Energies*, vol. 15, no. 6431, pp. 1–13, 2022.

[4] I. Fofana and A. Beroual, "A model for long air gap discharge using an equivalent electrical network," *IEEE Trans. Dielectr. Electr. Insul.*, vol. 3, no. 2, pp. 273–282, Apr. 1996.

[5] N. Monrolin, O. Praud, and F. Plouraboue, "Revisiting the positive DC corona discharge theory: Beyond peek's and Townsend's law," *Phys. Plasmas*, vol. 25, pp. 1–14, May 2018.

[6] B. Held and R. Peyrous, "Physical and chemical studies of corona discharges in air," *Czechoslovak J. Phys.*, vol. 49, no. 3, pp. 301–320, 1999.

[7] N. L. Allen, M. Abdel-Salam, and I. Cotton, "Effects of temperature and pressure change on positive corona and sparkover under direct voltage in short airgaps," *IET Sci., Meas. Technol.*, vol. 1, no. 4, pp. 210–215, Jul. 2007.

[8] E. B. Kulumbaev, V. M. Lelevkin, I. A. Niyazaliev, and A. V. Tokarev, "Characteristics of a corona discharge with a hot corona electrode," *Plasma Phys. Rep.*, vol. 37, no. 8, pp. 707–714, Aug. 2011.

[9] M. B. Awad and G. S. P. Castle, "Ozone generation in an electrostatic precipitator with a heated corona wire," *J. Air Pollut. Control Assoc.*, vol. 25, no. 4, pp. 369–374, Apr. 1975.

[10] N. L. Allen and J. C. P. Kong, "Positive corona inception in air at elevated temperatures," *IEE Proc.-Sci., Meas. Technol.*, vol. 153, no. 1, pp. 31–38, Jan. 2006.

[11] Y. Zheng, B. Zhang, and J. He, "Current-voltage characteristics of DC corona discharges in air between coaxial cylinders," *Phys. Plasmas*, vol. 22, no. 2, pp. 1–6, Feb. 2015.

[12] Z. Wang, T. Lu, Y. Liu, X. Bian, and X. Li, "Comparative study of two different measuring methods for corona current pulses," *J. Electrostatics*, vol. 88, pp. 134–138, Aug. 2017.

[13] R. G. Urban, H. C. Reader, and J. P. Holtzhausen, "Small corona cage for wideband HVac radio noise studies: Rationale and critical design," *IEEE Trans. Power Del.*, vol. 23, no. 2, pp. 1150–1157, Apr. 2008.

[14] B. Rakoshdas, "Pulses and radio-influence voltage of direct-voltage corona," *IEEE Trans. Power App. Syst.*, vol. PAS-83, no. 5, pp. 483–491, May 1964.

[15] J. P. Holtzhausen, P. J. Pieterse, and H. J. Vermeulen, "Investigation of the effect of conductor temperature on AC power line corona," in *Proc. Int. Conf. High Voltage Eng. Appl.*, New Orleans, LA, USA, Oct. 2010, pp. 96–99.

[16] G. J. Reid and H. J. Vermeulen, "Effects of conductor temperature on corona inception," in *Proc. 49th Int. Universities Power Eng. Conf. (UPEC)*, Cluj-Napoca, Romania, Sep. 2014, pp. 1–5.

[17] P. J. Pieterse, "Corona measurement in an inverted coaxial geometry to evaluate the effect of conductor temperature," in *Proc. South Africa Power Eng. Conf. (SAUPEC)*, Durban, South Africa, 2014, pp. 51–56.

[18] L. Liu, J. Guo, J. Li, and L. Sheng, "The effect of wire heating and configuration on ozone emission in a negative ion generator," *J. Electrostatics*, vol. 48, no. 2, pp. 81–91, Jan. 2000.

[19] S. Abdali and C. Aiane, "L'effet de la temperature sur les paramètres de la décharge couronne," Ph.D. dissertation, Departement de Génie électrique, Université Abderrahmane Mira-Bejaia, Béjaïa, Algeria, 2018.

[20] A. Yehia and A. Mizuno, "Ozone generation by negative direct current corona discharges in dry air fed coaxial wire-cylinder reactors," *J. Appl. Phys.*, vol. 113, no. 18, pp. 1–10, May 2013.

[21] M. Awad and G. P. Castle, "Breakdown streamers in coronas with heated discharge electrode," *IEEE Trans. Electr. Insul.*, vol. EI-12, no. 3, pp. 234–236, Jun. 1977.

[22] J.-R. Riba, M. Andrea, and F. Capelli, "Comparative study of AC and positive and negative DC visual corona for sphere plane gaps in atmospheric air," *Energies*, vol. 11, no. 2671, pp. 1–18, 2018.

[23] V. L. Chartier and R. D. Stearns, "Examination of grizzly mountain database to determine effects of relative air density and conductor temperature on HVDC corona phenomena," *IEEE Trans. Power Del.*, vol. 5, no. 3, pp. 1575–1582, Jul. 1990.

[24] V. L. Chartier, R. D. Stearns, and A. L. Burns, "Electrical environment of the uprated Pacific NW/SW HVDC intertie," *IEEE Trans. Power Del.*, vol. 4, no. 2, pp. 1305–1317, Apr. 1989.

[25] Y. Zebboudj and G. Hartmann, "Current and electric field measurements in coaxial system during the positive DC corona in humid air," *Eur. Phys. J.-Appl. Phys.*, vol. 7, no. 2, pp. 167–176, Aug. 1999.

[26] J. D. Cobine, "Glow discharges," in *Gaseous Conductors: Theory and Engineering Applications*, 1st ed., New York, NY, USA: Dover, 1958, pp. 205–289.

[27] P. Yan, C. Zheng, G. Xiao, X. Xu, X. Gao, and Z. C. K. Luo, "Characteristics of negative DC corona discharge in a wire-plate configuration at high temperatures," *Separat. Purification Technol.*, vol. 139, pp. 5–13, 2015.

[28] M. Abdel-Salam, M. Nakano, and A. Mizuno, "Corona-induced pressures, potentials, fields and currents in electrostatic precipitator configurations," *J. Phys. D, Appl. Phys.*, vol. 40, no. 7, pp. 1919–1926, Apr. 2007.

[29] Q. Chen, M. Fang, J. Cen, and J. Liu, "Characteristic of DC discharge in wire–cylinder configuration under coal pyrolysis gas components at high temperatures," *RSC Adv.*, vol. 8, no. 40, pp. 22737–22747, 2018.

[30] J. H. Chen and J. H. Davidson, "Model of the negative DC corona plasma: Comparison to the positive DC corona plasma," *Plasma Chem. Plasma Process.*, vol. 23, pp. 83–102, Jan. 2003.
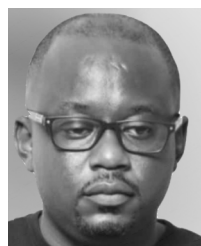
KAYUMBA G. ILUNGA received the B.Sc. degree in electromechanical engineering from the Universit de Lubumbashi, Congo, in 2009, and the M.Sc. degree in electrical engineering from the University of KwaZulu Natal, Durban, South Africa, in 2015, where he is currently pursuing the Ph.D. degree in electrical engineering. Before his academic pursuits, he gained professional experience as a Process Engineer with Brassimba, a renowned brewery in Lubumbashi, Congo, until 2012. In 2015, he was a Research Assistant with the Eskom Centre of Excellence, University of KwaZulu Natal. Additionally, from 2016 to 2019, he contributed as a Lecturer in computer science with the University of Kamina, Congo. His research interests include high voltage engineering, corona discharges, and conductor temperature.

ANDREW G. SWANSON received the degree in electrical engineering from the University of the Witwatersrand. He is currently a Senior Lecturer with the University of KwaZulu-Natal and a Professionally Registered Engineer. He has worked in the industry as an Engineering Consultant on railways, including 3 kV DC and 25 kV AC traction power systems, earthing and bonding of railways systems, compliance with power quality standards, and low voltage systems for stations and line side equipment. He is currently responsible for research and testing in the field of high voltage engineering and has tested overhead line equipment with voltages up to 350 kV ac, 650 kV impulse, and 350 kV dc according to the required high voltage standards.

NELSON MUTATINA IJUMBA (Senior Member, IEEE) received the B.Sc. degree (Hons.) from the University of Dar Es Salaam, Dar Es Salaam, Tanzania, in 1977, the M.Sc. degree from the University of Salford, Salford, U.K., in 1979, and the Ph.D. degree in electrical engineering from the University of Strathclyde, Glasgow, U.K., in 1987. He is currently an Emeritus Professor in electrical engineering with African Centre of Excellence in Energy for Sustainable Development (ACEESD), University of Rwanda, and a Honorary Professor in electrical engineering with the University of KwaZulu Natal, South Africa, where he was a Deputy Vice-Chancellor, a Researcher, and a Professor in electrical engineering. He is also a Practicing Engineer, a Chartered Engineer of the United Kingdom Engineering Council, a Registered Engineer in Tanzania, Kenya, and a Professional Engineer with the Engineering Council of South Africa. He is a fellow of the Southern African Institution of Electrical Engineers and a member of the Institution of Engineering and Technology. He has over 40 years of experience in teaching, research, consulting, and academic leadership. His research and consultancy services include the exploitation of green energy, renewable energy resources, energy efficiency, electrical power systems, high voltage technology, innovation, higher education management, and engineering education. He is passionate about the impact of technologies on sustainable development and translating research outputs into socially relevant innovative products. He has published widely in indexed journals and made numerous presentations at international and local conferences.

ROBERT STEPHEN was born in Johannesburg, South Africa. He received the B.Sc. degree in electrical engineering from the University of the Witwatersrand, in 1979, and the M.Sc., M.B.A., and Ph.D. degrees in overhead line design. He joined Eskom, the electrical utility, in 1980. He is currently a Master Specialist with the Technology Group, Eskom, responsible for distribution and transmission technologies of all voltages covering both AC and DC and for the smart grid strategy for Eskom. He is actually affiliated with the University of KwaZulu Natal, and he is also a member of the Eskom EPEP Group, University of KwaZulu Natal. He is the past Chairperson of Cigre SC B2 on overhead lines, has held positions in CIGRE as a Special Reporter and Working Group Chairperson and has authored over 100 technical articles. He was elected as the International President of CIGRE, in 2016. He is also a fellow of the South African Institute of Electrical Engineers (SAIEE) and was elected as the Honorary Vice President, in 2005. He received the SAIEE President's Award, in 2016. He is also the Editor-in-Chief of the *CIGRE Science & Engineering Journal*.

• • •